Front propagation in laminar flows

M. Abel[a,d], A. Celani[b], D. Vergni [a,c] and A. Vulpiani [a,c]

[a] Dipartimento di Fisica, Universitá di Roma "La Sapienza"

Piazzale Aldo Moro 2, I-00185 Roma, Italy

[b] CNRS, INLN, 1361 Route des Lucioles , F-06560 Valbonne, France.

[c] INFM unità di Roma "La Sapienza" Piazzale Aldo Moro 2, I-00185 Roma, Italy

[d] University of Potsdam, 14469 Potsdam, Germany

Abstract

The problem of front propagation in flowing media is addressed for laminar velocity fields in two dimensions. Three representative cases are discussed: stationary cellular flow, stationary shear flow, and percolating flow. Production terms of Fisher-Kolmogorov-Petrovskii-Piskunov type and of Arrhenius type are considered under the assumption of no feedback of the concentration on the velocity. Numerical simulations of advection-reaction-diffusion equations have been performed by an algorithm based on discrete-time maps. The results show a generic enhancement of the speed of front propagation by the underlying flow. For small molecular diffusivity, the front speed V_f depends on the typical flow velocity U as a power law with an exponent depending on the topological properties of the flow, and on the ratio of reactive and advective time-scales. For open-streamline flows we find always $V_f \sim U$, whereas for cellular flows we observe $V_f \sim U^{1/4}$ for fast advection, and $V_f \sim U^{3/4}$ for slow advection.

I. INTRODUCTION

Interface motion and front propagation in fluids occur in many different areas of interest to science and technology. Among the most important examples we mention chemical reaction fronts in liquids, population dynamics of ecological communities (e.g. plankton in the ocean), atmospheric chemistry (ozone hole) and flame propagation in gases [1].

The mathematical description of those phenomena is based on partial differential equations (PDE) for the evolution of the concentration of the reacting species and the evolution of the velocity field [2]. In principle the two PDEs (for the reactants and the velocity field) are coupled, often in a nontrivial way. An example is given by a recent study of reactants coupled to the Navier-Stokes equation by a Boussinesq term [3]. A mathematical simplification can be obtained assuming that the reactants do not influence the velocity field which evolves independently. In such a limit the dynamics is still completely nontrivial and it is described by a so-called advection-reaction-diffusion equation. In the most compact model one considers a single scalar field $\theta(\mathbf{x}, t)$, which represents the fractional concentration of products. The field θ has a zero value in the regions containing fresh material only, θ is unity where the reaction is over and there are only inert products left. In the region where the production takes place and reactants and products co-exist, the field θ assumes intermediate values.

The evolution of θ in a reacting fluid with molecular diffusivity D_0 is described by the PDE

$$\frac{\partial}{\partial t}\theta + (\mathbf{u} \cdot \nabla)\theta = D_0 \nabla^2 \theta + \frac{1}{\tau_r} f(\theta) \tag{1}$$

where $\mathbf{u}(\mathbf{x}, t)$ is an incompressible velocity field. The second term on the r.h.s. of Eq. (1) describes the production process, characterized by a typical time τ_r. The shape of $f(\theta)$ depends on the phenomenon under investigation, and we will consider two relevant functional forms:

1) $f(\theta) = \theta(1 - \theta)$, or more generally any convex function ($f''(\theta) < 0$) such that $f(0) = f(1) = 0$, $f'(0) > 0$ and $f'(1) < 0$. This is called the Fisher-Kolmogorov-

Petrovskii-Piskunov (FKPP) nonlinearity [4]. The production term is proportional to the concentration of reactants, $1 - \theta$, and to the concentration of products, θ.

2) $f(\theta) = e^{-\theta_c/\theta}(1 - \theta)$. This is the Arrhenius nonlinearity [5]. In this case, the solution $\theta = 0$ is only marginally unstable, and the parameter θ_c plays the role of an activation concentration, since practically no production takes place for products concentrations below that threshold. Production is still proportional to the concentration of fresh material.

We will always consider initial conditions such that $\theta(\mathbf{x}, 0) \to 1$ exponentially fast as x, the horizontal coordinate, approaches $-\infty$, and $\theta(\mathbf{x}, 0) \to 0$ exponentially fast as $x \to \infty$. The initial profile of θ has no variation along the transversal axis. The choice of such an initial condition, for which the concentration of products has a noncompact support, is of interest because it suppresses all possible flame-quenching effects that may appear in case 2) (see e.g. [6]). This allows a direct comparison between FKPP and Arrhenius production terms. There exists a huge literature for the case $\mathbf{u} = 0$ (see e.g. [5]). In that case the physical mechanism for front propagation resides in the the combined effect of diffusion and production. Let us indeed consider a one-dimensional situation where a reservoir of fresh material is located on the right side, whereas on the opposite side we have only inert products. At the boundary between the two phases, diffusion mixes fresh material and inert products, broadening the interface. Then, production raises the level of the concentration of products, thus shifting the interface, to the right in this case. The final result is a front propagating from left to right, eating out fresh material to leave behind digested, inert products. The front speed at large times reaches a limiting value V_0. For the FKPP nonlinearity one has the exact result

$$V_0 = 2\sqrt{\frac{D_0 f'(0)}{\tau_r}} \tag{2}$$

whereas for a generic $f(\theta)$ one has the bounds [4,5,7]

$$2\sqrt{\frac{D_0}{\tau_r} f'(0)} \leq V_0 \leq 2\sqrt{\frac{D_0}{\tau_r} \sup_\theta \frac{f(\theta)}{\theta}} \; . \tag{3}$$

3

It has to be remarked that the convergence to the limiting velocity is extremely slow for FKPP production [8,9], therefore this case requires special attention especially for nonuniform flow.

In the presence of a moving medium, i.e. $\mathbf{u} \neq 0$, one expects that the front propagates with an average limiting speed V_f. A problem of primary interest is to determine the dependence of V_f on the properties of the velocity field $\mathbf{u}$ [10,11]. In this article we consider front propagation in simple laminar flows (shear flow and systems with cellular structures) which, in spite of their apparent simplicity, show intriguing behaviour [12–15]. For a given structure of the flow field, we aim to explore the dependence of V_f on relevant parameters, such as the typical flow velocity U and the production time-scale τ_r. In terms of adimensional quantities, we look for an expression for the speed enhancement V_f/V_0 in terms of the *Damköhler number*, $Da = L/(U\tau_r)$, which measures the ratio of advective to reactive time-scales, and in terms of the *Péclet number*, $Pe = UL/D_0$ which expresses the relative weight of advection and diffusion. We will mainly be interested in the case of large Pe, to highlight the combined effects of advection and reaction. The two regimes $Da \ll 1$ and $Da \gg 1$ are quite different in nature: in the first case, typical for slow reaction rates or fast advection, the front interface is distributed over several length-scales L, and for this reason it goes under the name of "distributed reaction zone" regime [16]; in the second case, the front is thin compared to L, and it propagates according to a Huyghens-like principle, hence the name of "geometrical optics" regime [16]. We will provide a detailed analysis of these two regimes, highlighting their differences. In the context of the thin front regime we can mention, among the many contributions, the works on the G-equation approximation and its relation with the "geometrical optics" regime [19,20], the work on turbulent flows [10,11] and the numerical study of front propagation in synthetic turbulence [23].

A hint to the effect of an underlying flow on front propagation is given by the observation that the front speed increases with the square-root of molecular diffusivity. It is well-known that diffusive transport is always enhanced by incompressible flow, resulting in an effective diffusion coefficient $D_{\text{eff}} > D_0$ [27,32,33]. Therefore, it is reasonable to expect that the front

speed will be enhanced, too. This physical argument can be upgraded to a mathematically rigorous statement in the case of a "slow" reaction, that is for $Da \ll 1$ (see Section II). From the mathematical viewpoint, there exist lower bounds to the speed of the front which confirm the expectation that the flow enhances front propagation [17,18]. These bounds take different forms according to the topological structure of the flow field. One can distinguish two main classes: cellular flows, characterized by having closed streamlines only, and percolating flows, which possess open streamlines (shear flows are a particular case of this second class, having only open streamlines). For cellular flows, it has been shown that $V_f/V_0 \geq C_1 Da^{-1/2} + C_2$ for $Da \geq 1$ and $V_f/V_0 \geq C_1 Da^{-1/5} + C_2$ for $Da \leq 1$, with constants C_1, C_2 depending on the shape of the production term. For percolating flows, the lower bound is expressed as $V_f \geq K_1 U$ where again K_1 is a constant depending on f. The most general upper bound, valid for flows of both classes, is $V_f \leq V_0 + K_2 U$ [17]. We therefore see that percolating flows are constrained to a linear dependence on the stirring intensity U (see Section IV A for numerical results). Cellular flows have more intriguing properties, as we will see in Section IV B: for fast advection, $Da \ll 1$, the front speed depends on the flow velocity as $V_f \propto U^{1/4}$, to be compared with the lower bound prediction $\propto U^{1/5}$ and the upper bound $\propto U$; for slow advection, $Da \gg 1$, we obtain $V_f \propto U^{3/4}$ to compare with the lower bound $\propto U^{1/2}$ and the upper bound $\propto U$. It is clear that these bounds do not provide a sharp evaluation of the front speed in the case of a cellular flow.

To close the overview of mathematical results, we anticipate that a different upper bound for the front speed enhancement can be obtained by reformulating the solutions of Eq. (1) in terms of a path-integral (see Section II for details, and references therein). This bound yields an expression similar to the one obtained in the absence of any flow, but with an effective diffusion coefficient D_{eff} replacing the molecular one. Explicitly, we show that

$$V_f \leq 2\sqrt{\frac{D_{\text{eff}}}{\tau_r} \sup_{\theta} \frac{f(\theta)}{\theta}} \tag{4}$$

where the dependence of D_{eff} on the flow parameters and on the molecular diffusion can be derived by the analysis of Eq. (1) when the production term has been switched off.

For a cellular flow, we have the result $D_{\text{eff}} \sim \sqrt{ULD_0}$, [14,13], whereas for a shear flow $D_{\text{eff}} \sim (UL)^2/D_0$ [30]. Inserting these latter expressions in Eq. (4) we obtain the behaviour $V_f \propto U^{1/4}$ for the cellular flow $--$ also obtained by [36] $--$ and $V_f \propto U$ for the shear flow, remarkably close to the observed ones for $Da \ll 1$. Furthermore, the upper bound (4) is sharp in the regime where homogenization techniques apply (see Section II and Appendix C). In other words, for fast advection the effect of the underlying flow can be compactly expressed in the renormalization of the diffusion coefficient. On the contrary, for slow advection in a cellular flow, the front speed departs significantly from the upper bound, with an increase in front speed less prominent than in the fast advection regime. We will see in Section IV B that the main physical mechanism accounting for this depletion is the appearance of an effective reaction term as a consequence of the joint effect of advection and reaction.

These observations lead us to argue that the effect of a stirring velocity on front propagation can be in general summarized in the renormalization of the two relevant parameters: *(i)* an effective diffusivity, which is always larger than the molecular one for an incompressible flow, and *(ii)* an effective production term, which is slower than the microscopic one for slow advection.

The remainder of the paper is organized as follows: in Section II, we derive some general results valid for *all* advecting flows; Section III presents the algorithm employed for the numerical solution of Equation (1); in Section IV we discuss the results of numerical simulations; Section V is devoted to conclusions and discussion. Technical and numerical details are treated in the Appendices.

II. UPPER BOUNDS TO FRONT SPEED

In this Section we show how to establish the upper bound (4) for the speed of front propagation in a generic incompressible flow and a generic production term. This result is the consequence of the deeply rooted link existing between front propagation and advective transport. In other words, we will exploit the relationship of the solutions of Eq. (1) to the solutions of

the same equations in absence of production terms. This will yield the constraint (4) involving the front speed V_f, the effective diffusion coefficient D_{eff} and the production time-scale τ_r. In general this relation is an inequality, and not a sharp functional relation. In a graphical form, this amounts to say that "front propagation$\neq$(advection+diffusion)+production". A significant exception to this general rule is given by the limit of very slow reaction (or very fast advection), where the bound (4) becomes sharp. In this case, homogenization techniques, detailed in Appendix A, allow to show that the problem of the determination of the front speed reduces to the problem of determining D_{eff}. This is essentially due to the large separation of typical time-scales.

We start our proof of the inequality (4) by recalling the fundamental relation among the solution of the PDE (1) and the trajectories of particles advected by a velocity field $\mathbf{u}(\mathbf{x}, t)$ and subject to molecular diffusion [25,26]

$$\theta(\mathbf{x}, t) = \left\langle \theta(\mathbf{r}(0), 0) \, e^{\int_0^t c(\theta(\mathbf{r}(s), s)) \mathrm{d}s} \right\rangle_\eta \tag{5}$$

where

$$c(\theta) = \frac{1}{\tau_r} \frac{f(\theta)}{\theta}$$

is the growth rate of θ. The average is performed over the trajectories evolving according to the Langevin equation

$$\frac{d\mathbf{r}(t)}{dt} = \mathbf{v}(\mathbf{r}(t), t) + \sqrt{2D_0} \boldsymbol{\eta}(t) \tag{6}$$

with final conditions $\mathbf{r}(t) = \mathbf{x}$. The white noise term $\sqrt{2D_0} \boldsymbol{\eta}(t)$ accounts for molecular diffusion.

Since the growth rate is always bounded from above, $c(\theta) \leq c_{\text{max}} \equiv \sup_\theta c(\theta)$, Eq. (5) yields the inequality

$$\theta(t, \mathbf{x}) \leq \langle \theta(0, \mathbf{r}(0)) \rangle \exp(c_{\text{max}} t) \ . \tag{7}$$

For FKPP production terms the maximum occurs for $\theta = 0$, that is we have $c(\theta) \leq c(0) = f'(0)/\tau_r = 1/\tau_r$, therefore $c_{\text{max}} = 1/\tau_r$. In the inequality (7), the term in an-

gular brackets denotes the probability that the trajectory ending at $\mathbf{x}$ were initially located at the left of the front interface. Under very broad conditions, i.e. nonzero molecular diffusivity and finite variance of the velocity vector potential [27,32,33], it is possible to show that asymptotically the particles undergo a normal diffusion process with an effective diffusion coefficient D_{eff}, always larger than the molecular value D_0. This is the rigorous and most general version of a statement originally due to Taylor [34]. The issue of single particle diffusion, and the problem of finding the effective diffusivity, given a velocity field and a molecular diffusivity, has been the subject matter of a huge amount of work (see e.g. [35] for a recent review). In the presence of an asymptotic normal diffusion, we can substitute the term $\langle \theta(0, \mathbf{r}(0) \rangle$, with the gaussian result $1 - \frac{1}{2}\text{erfc}(-x/\sqrt{2D_{\text{eff}}t}) \simeq \exp[-x^2/(4D_{\text{eff}}t)]/\sqrt{2\pi D_{\text{eff}}t}$, where the latter approximation holds with exponential accuracy. We thus obtain $\theta(t, \mathbf{x}) \leq \exp\left[c_{\max}t - x^2/(4D_{\text{eff}}t)\right]/\sqrt{2\pi D_{\text{eff}}t}$. It is therefore clear that at the point $\mathbf{x}$ the field θ is exponentially small until a time t of the order of $x/\sqrt{4D_{\text{eff}}c_{\max}}$. We therefore obtain the upper bound for the front velocity $V_f \leq \sqrt{4D_{\text{eff}}c_{\max}}$, as anticipated in Eq. (4).

The analytic determination of the effective diffusivity from the knowledge of the advecting field and the value of the molecular diffusivity is – in general – a daunting task. Nevertheless there is an exact result valid for all flows in the form of an upper bound for the effective diffusivity $D_{\text{eff}} \leq D_0(1 + \alpha Pe^2)$, where α is a numerical constant that depends on the details of the flow [27,32,33]. Plugging this relation into (4) we can derive a general upper bound

$$V_f/V_0 \leq \sqrt{1 + \alpha Pe^2} \tag{8}$$

where any dependence on the flow details has been summarized in the numerical constant α. For large Pe we recover the bound $V_f \leq \text{const.}\dot{U}$ already discussed in Ref. [17]. In the limit of small Pe, i.e. for small stirring intensity U, this bound is in agreement with the Clavin-Williams relation $(V_f - V_0)/V_0 = (U/V_0)^2$ [10]. On the contrary, in the same limit, an asymptotic behavior like $(V_f - V_0)/V_0 \sim (U/V_0)^{4/3}$, proposed in Ref. [11], is ruled out since the rate of convergence to V_0 for vanishing U has to be faster or equal to U^2 in order

to fulfill the bound (8).

As anticipated above, there is a situation where the bound (4) becomes sharp, and that is the limit of very slow reaction. It is easy to understand the physical reasons for this effect. If τ_r is the slowest time-scale under consideration, advection and molecular diffusion act jointly to build an effective diffusion process, unaffected by reaction. Diffusion decreases the value of concentration to lower levels before the onset of production, which then takes place at the maximal rate (e.g., for FKPP, at $\theta \simeq 0$). In the limit of very slow reaction, basically one has that Eq. (1), at large scale and long time, behaves as a reaction-diffusion equation (i.e. with $\mathbf{u} = 0$) where D_0 is replaced by D_{eff}. Therefore for FKPP nonlinearity, using Eq. (2) one has: $V_f \simeq 2\sqrt{\frac{D_{\mathrm{eff}}}{\tau_r}}$. For a detailed derivation of this statement, the reader is referred to the Appendix A.

III. A DISCRETE-TIME APPROACH

Let us now briefly discuss the general idea of our numerical approach to the study of front dynamics in terms of discrete-time maps.

The physical meaning of Eq. (5) is made clear by the limit $D_0 = 0$. In that case, introducing the Lagrangian time derivative

$$\frac{\mathrm{D}}{\mathrm{D}t} = \frac{\partial}{\partial t} + \mathbf{u} \cdot \nabla \ .$$

Eq. (1) reduces to

$$\frac{\mathrm{D}}{\mathrm{D}t}\theta = \frac{1}{\tau_r} f(\theta) \ . \tag{9}$$

Denoting by $\mathbf{F}^t$ the formal evolution operator of Eq. (6) without noise ($D_0 = 0$), i.e. $\mathbf{x}(t) = \mathbf{F}^t \mathbf{x}(0)$, and by G^t the evolution operator of $\frac{\mathrm{d}}{\mathrm{d}t}\theta = \frac{1}{\tau_r} f(\theta)$, i.e. $\theta(t) = G^t \theta(0)$, one can write the solution of Eq. (9) in the form:

$$\theta(\mathbf{x}, t) = G^t \theta(\mathbf{F}^{-t}\mathbf{x}, 0) \ . \tag{10}$$

Equation (10) is nothing but Eq. (5) in the absence of molecular diffusivity, i.e. when only one path ends in $\mathbf{x}$ at time t.

In the following, we will concentrate on laminar velocity fields and we will develop a suitable framework to compute some essential properties for these systems. In time-periodic velocity fields, $\mathbf{u}(\mathbf{x}, t+\Delta t) = \mathbf{u}(\mathbf{x}, t)$ where Δt is the period and for $D_0 = 0$ the Lagrangian motion can be described by a discrete-time dynamical system. In other words, the position $\mathbf{x}(t + \Delta t)$ is univoquely determined by $\mathbf{x}(t)$; in addition, because of the time-periodicity, the map $\mathbf{x}(t) \to \mathbf{x}(t + \Delta t)$ does not depend on t. We remind that a periodic time dependence is sufficient to induce Lagrangian chaos [24].

With these considerations in mind, we can write a Lagrangian map for the position:

$$\mathbf{x}(t + \Delta t) = \mathbf{F}_{\Delta t}(\mathbf{x}(t)) . \tag{11}$$

If $\mathbf{u}$ is incompressible, the map (11) is volume preserving i.e. its Jacobian matrix has unit determinant. In the following we will limit our analysis to the bidimensional case. In that situation the map (11) is symplectic, and the dynamics is described by a discrete-time version of an Hamiltonian system. Of course it is not simple at all to find explicitly $\mathbf{F}_{\Delta t}(\mathbf{x})$ for a generic velocity field. On the contrary, it is not difficult to build $\mathbf{F}_{\Delta t}$ in such a way that the qualitative features of a given flow are well modeled, as we will show below.

Another situation in which one obtains exactly a discrete-time map (11) for the Lagrangian motion, is the case of velocity field which is always zero apart from δ-impulses at times $t = 0, \pm\Delta t, \pm 2\Delta t, \pm 3\Delta t, \ldots$

$$\mathbf{u}(\mathbf{x}, t) = \sum_{n=-\infty}^{\infty} \mathbf{v}(\mathbf{x})\delta(t - n\Delta t) . \tag{12}$$

The effects of a non zero diffusivity are taken into account by adding a noise term

$$\mathbf{x}(t + \Delta t) = \mathbf{F}_{\Delta t}(\mathbf{x}(t)) + \sqrt{2D_0\Delta t}\, \mathbf{w}(t) , \tag{13}$$

where $\mathbf{w}(t)$ are standard independent gaussian variables.

If the production term also is zero apart from δ-impulses

$$f(\theta) = \sum_{n=-\infty}^{\infty} g(\theta)\delta(t - n\Delta t) , \tag{14}$$

10

one can introduce a reaction map

$$\theta(t + \Delta t) = G_{\Delta t}(\theta(t)) \ . \tag{15}$$

Now we are ready to write the dependence of the field θ at time $t + \Delta t$ on the field at time t in terms of the advection and reaction maps, $\mathbf{F}_{\Delta t}$ and $G_{\Delta t}$

$$\theta(\mathbf{x}, t + \Delta t) = \left\langle G_{\Delta t}(\theta(\mathbf{F}_{\Delta t}^{-1}(\mathbf{x} - \sqrt{2D_0 \Delta t}\, \mathbf{w}(t)), t)) \right\rangle_{\mathbf{w}} \tag{16}$$

Equation (16) is exactly equivalent to Eq. (5) for maps (for velocity field and reaction given by periodic δ-impulses).

The concentration field just after the kick, $\theta(\mathbf{x}, t + 0)$, can be written as

$$\theta(\mathbf{x}, t + 0) = G_{\Delta t}\left(\theta(\mathbf{F}_{\Delta t}^{-1}(\mathbf{x}), t)\right) \ . \tag{17}$$

The concentration field $\theta(\mathbf{x}, t + \Delta t - 0)$ is obtained from $\theta(\mathbf{x}, t + 0)$ solving the bare diffusion equation $\partial_t \theta = D_0 \nabla^2 \theta$ with the initial condition given by Eq. (17):

$$\theta(\mathbf{x}, t + \Delta t - 0) = \frac{1}{(2\pi)^{d/2}} \int e^{-\frac{w^2}{2}} \theta(\mathbf{x} - \sqrt{2D_0 \Delta t}\, \mathbf{w}, t + 0) \, d\mathbf{w} \ , \tag{18}$$

which is nothing but Eq. (16), and d is the dimension of the space, $\mathbf{x} \in \mathbb{R}^d$.

From an algorithmic point of view the whole process between t and $t + \Delta t$ can be thus divided into three steps, a diffusive, an advective and a reactive one. The first two steps determine the origin of the Lagrangian trajectory ending in $\mathbf{x}$ and accordingly have to evolve backwards in time with a given noise realization $\mathbf{w}$. In the third step, the reaction at the point $\mathbf{x}$ for the advected/diffused passive scalar θ is computed:

1) backward diffusion: $\mathbf{x} \rightarrow \mathbf{x} - \sqrt{2D_0 \Delta t}\, \mathbf{w}$

2) backward advection via the Lagrangian map: $\mathbf{x} - \sqrt{2D_0 \Delta t}\, \mathbf{w} \rightarrow \mathbf{F}^{-1}(\mathbf{x} - \sqrt{2D_0 \Delta t}\, \mathbf{w})$

3) forward reaction: $\theta(t + \Delta t) = G_{\Delta t}(\theta(t))$.

Let us remark that Eq. (16) is exact if both the velocity field and the reaction are δ-pulsed processes. However one can also use the formula (16) as a practical method for the numerical

11

integration of Eq.(1) if one assumes small enough Δt, so that the Lagrangian and reaction maps are given at the lowest order by

$$\mathbf{F}_{\Delta t}(\mathbf{x}) \simeq \mathbf{x} + \mathbf{u}(\mathbf{x})\Delta t \ , \qquad G_{\Delta t} \simeq \theta + \frac{\Delta t}{\tau_r}f(\theta) \ .$$

A. The choice of the reaction map

We now introduce a reaction map $G_{\Delta t}(\theta)$ corresponding to FKPP nonlinearity. The map is characterized by an unstable fixed point in $\theta = 0$, a stable one in $\theta = 1$, and a convex shape:

$$G_{\Delta t}(\theta) = (1 + \alpha\Delta t)\theta + O(\Delta t\,\theta^2) \qquad \text{for } \theta \simeq 0$$

$$G_{\Delta t}(\theta) = 1 - \beta\Delta t(1 - \theta) + O(\Delta t(1 - \theta)^2) \qquad \text{for } \theta \simeq 1$$

Similarly, for the Arrhenius case we define

$$G_{\Delta t}(\theta) = \theta + O(\Delta t\, e^{-\theta_c/\theta}) \qquad \text{for } \theta \simeq 0$$

$$G_{\Delta t}(\theta) = 1 - \beta\Delta t(1 - \theta) + O(\Delta t(1 - \theta)^2) \qquad \text{for } \theta \simeq 1 \ ,$$

(see Figure 1). We expect from known results [5], for the time-continuous PDE (1) that at a qualitative level, the details in the shape of $G_{\Delta t}(\theta)$ are not very relevant, within a given class of nonlinearities (e.g. FKPP). This expectation is confirmed by numerical simulations. Naturally, if one is interested in the details of some specific combustion processes, one has to work with a precise shape of $G_{\Delta t}$.

B. The choice of the lagrangian map

If we limit our study to the 2D case, the incompressibility of the velocity field implies symplecticity of the map (11). A rather general class of symplectic maps is the following:

$$\begin{cases} x(t + \Delta t) = x(t) + p_{\Delta t}(y(t)) \\ y(t + \Delta t) = y(t) + q_{\Delta t}(x(t + \Delta t)) \ . \end{cases} \tag{19}$$

It is easy to verify that (19) is symplectic for any choice of $p_{\Delta t}(\cdot)$ and $q_{\Delta t}(\cdot)$. If $p_{\Delta t}(y) = k\,\Delta t\,\sin y$ and $q_{\Delta t}(x) = k\,\Delta t\,\sin x$ one has the so called Harper model (often studied in the quantum chaos context) corresponding to a chaotic transport in spatially periodic cellular structures. The case $q_{\Delta t}(x) = 0$ gives a non-chaotic shear flow in the x direction. The celebrated standard map [38], which is a paradigmatic model for chaotic behaviour in low dimensional Hamiltonian system, is obtained with $p_{\Delta t}(y) = k\,\Delta t\,\sin y$ and $q_{\Delta t}(x) = x$.

In the following we will study two limit cases which give nonchaotic transport, i.e. the role of the molecular diffusivity is very important:

a) open flow field (shear flow) where all the streamlines are open

b) convective rolls where all the streamlines are closed.

For the shear flow, we set $q_{\Delta t}(x) = 0$ in (19), as mentioned above. For the cellular flows we have built the Lagrangian map in the following way: consider a 2d incompressible steady velocity field $\mathbf{u}(x, y) = (-\partial_y \psi(x, y), \partial_x \psi(x, y))$ generated by the streamfunction

$$\psi(x, y) = UL \sin(\frac{2\pi x}{L}) \sin(\frac{2\pi y}{L}) \ , \tag{20}$$

with L-periodic conditions in y and infinite extent along the x-axis. The Lagrangian map $\mathbf{F}_{\Delta t}(\mathbf{x})$ is given by the exact integration of the equation $\frac{\mathrm{d}}{\mathrm{d}t}\mathbf{x} = \mathbf{u}(\mathbf{x})$ on an interval Δt. The shape of $\mathbf{F}_{\Delta t}(\mathbf{x})$, i.e. the expression of $\mathbf{x}(t + \Delta t)$ as a function of $\mathbf{x}(t)$ is found explicitly in terms of elliptic functions.

In addition to the cases a) and b) we will study the relevance of a "transversal" perturbation to the shear flow.

IV. NUMERICAL RESULTS

Since we are interested in the front propagation in one direction, say the x-direction, we applied in our simulations periodic boundary conditions in y-direction:

$$\theta(x, y, t) = \theta(x, y + L_y, t) \tag{21}$$

13

whereas in x-direction we have

$$\lim_{x \to \infty} \theta(x, y, t) = 0 , \tag{22}$$

$$\lim_{x \to -\infty} \theta(x, y, t) = 1 . \tag{23}$$

In this way the front propagates from left to right.

The instantaneous front speed $V(t)$ is defined by

$$V(t) = \frac{1}{\Delta t L_y} \int \int dx \, dy [\theta(x, y, t + \Delta t) - \theta(x, y, t)] . \tag{24}$$

Since $V(t)$ in general shows some oscillations in time, one can define the mean front speed V_f by the time average over a sufficiently long time, after the transient.

The numerical implementation of the formula (16) is described in detail in Appendix C.

We have first checked the numerical code to confirm the known results for the front speed V_f in the case of FKPP nonlinearity:

i) only molecular diffusion is present, i.e. $\mathbf{F(x)} = \mathbf{x}$. In this case, equivalent to $\mathbf{u} = \mathbf{0}$, one has the discrete time version of the FKPP formula (2)

$$V_f = \frac{2}{\Delta t} \sqrt{D_0 \Delta t \, \ln\left(G'_{\Delta t}(0)\right)} . \tag{25}$$

See Appendix B for its derivation.

ii) the reaction is very slow, i.e., $\tau_r = \Delta t / \ln(G'_{\Delta t}(0)) \gg t_a$ (where t_a is the advection time). In this case homogenization techniques can be applied (see e.g. [17], and Appendix A) and one finds

$$V_f \simeq \frac{2}{\Delta t} \sqrt{D_{\text{eff}} \, \Delta t \, \ln\left(G'_{\Delta t}(0)\right)} = 2\sqrt{\frac{D_{\text{eff}}}{\tau_r}} . \tag{26}$$

The effective Diffusion coefficient D_{eff} in the x-direction is defined by

$$D_{\text{eff}} = \lim_{t \to \infty} \frac{\langle (x(t) - x(0))^2 \rangle}{2t} \tag{27}$$

14

and in general must be computed numerically iterating the map (13).

In order to show the validity of the homogenization limit (26) we consider a system where the lagrangian motion is given by the standard map

$$\begin{cases} x(t+1) = x(t) + K\sin(y(t)) \\ y(t+1) = y(t) + x(t+1) \quad \text{mod } 2\pi , \end{cases} \tag{28}$$

and the reaction map $G(\theta)$ is in the FKPP class

$$G(\theta) = \theta + c\theta(1-\theta) \qquad \text{if } c \le 1 . \tag{29}$$

In the case of $c > 1$, in order to avoid unbounded reaction map, we use

$$G(\theta) = \begin{cases} \theta + c\theta(1-\theta) & \text{for} \quad \theta \le \theta^* \\ 1 - \alpha(1-\theta) & \text{for} \quad \theta > \theta^* , \end{cases} \tag{30}$$

where $\theta^* = (c + 2 - \sqrt{c^2 + 4})/2c$ and $\alpha = (c + 2 - \sqrt{c^2 + 4})/(c - 2 + \sqrt{4 + c^2})$.

By varying c one can change the ratio between the advection time $t_a \sim O(1)$ and the reaction time $\tau_r = \frac{1}{\ln G'(0)} = \frac{1}{\ln(1+c)}$, i.e. the Damköhler number. Figure 2 shows V_f vs $1/c$, for $K = 1$ and $K = 3$. At large τ_r, i.e. large c^{-1} the homogenization limit is recovered.

We now move to the description of the numerical results in three case studies.

A. Shear Flow

The shear flow is the simplest case to study and it will be presented here shortly. For our simulations we use the system (19) with $q = 0$:

$$\begin{cases} x(t+1) = x(t) + U\sin(2\pi y(t)/L_y) \\ y(t+1) = y(t) . \end{cases} \tag{31}$$

and a reaction map $G(\theta)$ of the shape (29) (30), where for the sake of simplicity we use $\Delta t = 1$. While keeping fixed the diffusivity we investigate the different regimes in the (U, τ_r) space. Among all the possible combinations of diffusion, advection and reaction time scales,

15

we assume in this paper always that diffusion is the slowest one.

The front velocity in the homogenization regime, i.e. very slow reaction, is $V_f \simeq 2\sqrt{\frac{D_{\text{eff}}}{\tau_r}}$, where D_{eff} can be easily computed for the shear flow [30]: $D_{\text{eff}} - D_0 \sim U^2/D_0$. Therefore for slow reaction one has a linear behaviour $V_f \sim U$. The bounds discussed in the introduction suggest that in general $V_f = aU + b$ where a and b may depend on τ_r and D_0, as confirmed by recent numerical results [31].

In Fig. 3 we show two snapshots of the concentration field for slow and fast reaction. In Fig. 4 the front velocity is displayed in dependence on the advection velocity U for different reaction times. homogeneization holds for slow reaction rates; decreasing τ_r the front speed increases until for high reaction rates the geometrical optics regime is reached.

Our results obtained with the discrete time map approach are in perfect agreement with the direct numerical simulations presented in Ref. [31], where the dynamical equations are solved in the Eulerian framework.

B. Cellular Flow

The numerical simulations have been performed using the velocity field $\mathbf{u}(x,y) = (-\partial_y\psi(x,y), \partial_x\psi(x,y))$ generated by the streamfunction defined in Eq. (20) and $G(\theta)$ given by (29) and (30) with $c = \Delta t/\tau_r$ and $\Delta t \ll \tau_r$. In Fig. 5 we show a snapshot of the concentration field for two values of τ_r.

The key to the understanding of the different regimes of front propagation stands in the description of front dynamics in terms of effective macroscopic equations, which we introduce hereafter, following Ref. [36]. The dynamics of θ is characterized by the length-scale of the cell-size, L. We can therefore perform a space discretization which reduces each cell, C_i, to a point, i, mapping the domain – a two-dimensional infinite strip – to a one-dimensional lattice, and the field θ to a function defined on the lattice $\Theta_i = L^{-2}\int_{C_i}\theta\,dx\,dy$. Integrating Eq. (1) over the cell C_i we obtain $\dot{\Theta}_i = J_{i+1} - J_i + \chi_i$ where $J_i = L^{-2}\int_{\text{left}}D_0\partial_x\theta\,dy$ is the flux of matter through the left boundary of the i-th cell, and $\chi_i = L^{-2}\int_{C_i}\tau_r^{-1}f(\theta)\,dx\,dy$ is

the rate of change of Θ_i due to reaction taking place within the cell. We will show that it is possible to model the dynamics with a space-discretized macroscopic reaction-diffusion equation:

$$\dot{\Theta}_i = D_{\text{eff}}(\frac{1}{2}\Theta_{i+1} - \Theta_i + \frac{1}{2}\Theta_{i-1}) + \tau_{\text{eff}}^{-1}F(\Theta_i)\,. \tag{32}$$

The effect of velocity is to *renormalize* the values of diffusivity, $D_0 \rightarrow D_{\text{eff}}(D_0, U, L)$, and reaction time-scale, $\tau_r \rightarrow \tau_{\text{eff}}(\tau_r, U, L)$ and therefore the advective term does not appear any longer in the effective dynamics given by Eq. (32). The assumption that κ and τ are independently renormalized by advection is consistent in the regime $v/U = (Da/Pe)^{1/2} \ll 1$ The renormalized diffusivity D_{eff} accounts for the process of diffusion from cell to cell resulting from the nontrivial interaction of advection and molecular diffusion. The renormalized reaction-time τ_{eff} amounts to the time that it takes to a single cell to be completely burned, and depends on the interaction of advection and production. In that context, the limiting speed of the front in the moving medium will be $V_f \simeq 2\sqrt{D_{\text{eff}}/\tau_{\text{eff}}}$. The goal is now to derive the expressions for the renormalized parameters from physical considerations.

Renormalization of diffusivity. To obtain the value of D_{eff} it is sufficient to neglect the reaction term in equation (1), i.e. consider a passive scalar in a cellular flow. The solution is known, [12–14],

$$\frac{D_{\text{eff}}}{D_0} \sim Pe^{1/2} \qquad Pe \gg 1\,. \tag{33}$$

For large Pe (D_0 small) the cell-to-cell diffusion mechanism can be qualitatively understood in the following way: the probability for a particle of the scalar to jump across the boundary of the cell, in a circulation time L/U, by virtue of molecular diffusion, can be estimated as the ratio of the diffusive motion across the streamlines, $O(\sqrt{D_0 L/U})$, to advective motion along streamlines, $O(L)$, leading to $p \sim (D_0/(UL))^{1/2}$, hence the effective diffusivity $D_{\text{eff}} \sim pUL \sim D_0 Pe^{1/2}$.

Renormalization of reaction time. At small Da, where reaction is significantly slower than advection, the cell is first invaded by a mixture of reactants and products (with a low content

17

of products, $\Theta_i \ll 1$) on the fast advective time-scale, and complete reaction ($\Theta_i = 1$) is then achieved on the slow time-scale $\tau_{\text{eff}} \simeq \tau_r$ (Figure 6). The area where the reaction takes place extends over several cells, i.e. the front is "distributed".

At large Da, the ratio of time-scales reverses, and in a (now short) time τ_r two well-separated phases emerge inside the cell. The interface has a depth $\lambda \sim \sqrt{D_0 \tau_r} = L Pe^{-1/2} Da^{-1/2}$, i.e. it is thin compared to the cell size. Here the process is characterized by an inward spiral motion of the outer, stable phase (see Figure 7), at a speed proportional to U as it usually happens for a front in a shear flow at large Da. Indeed it is easy to show that, inside a cell, the problem can be mapped to a front propagation in a shear-flow in "action-angle" variables [15]. Therefore the $\theta = 1$ phase fills the whole cell on the advective time-scale, giving $\tau_{\text{eff}} \simeq L/U$.

In summary, we have the following behavior for the renormalized reaction time

$$\frac{\tau_{\text{eff}}}{\tau_r} \sim \begin{cases} 1 & Da \ll 1 \\ Da & Da \gg 1 \ . \end{cases} \tag{34}$$

Now, we have all the information to derive the effective speed of front propagation for a cellular flow. Recalling that $V_f \sim \sqrt{D_{\text{eff}}/\tau_{\text{eff}}}$, we have for the front velocity the final result

$$\frac{V_f}{V_0} \sim \begin{cases} Pe^{1/4} & Da \ll 1, Pe \gg 1 \\ Pe^{1/4} Da^{-1/2} & Da \gg 1, Pe \gg 1 \end{cases} \tag{35}$$

where we restricted ourselves to the most interesting case $Pe \gg 1$. At small Da the front propagates with an effective velocity which scales as the upper bound derived above, that is as $Pe^{1/4}$. At large Da front speed is less enhanced than at small Da: according to Eq. (35), we have $V_f/\sqrt{4D_{\text{eff}}/\tau_r} \sim Da^{-1/2}$ for $Da \gg 1$. In terms of the typical velocity of the cellular flow, we have $V_f \propto U^{1/4}$ for "fast" advection ($U \gg L/\tau_r$, or equivalently $Da \ll 1$) whereas $V_f \propto U^{3/4}$ for "slow" advection ($U \ll L/\tau_r$, or $Da \gg 1$). The numerical results are shown in Figure 8. The case of "fast" advection corresponds to the one with slow reaction, for which the homogenization limit holds.

In the geometrical optics limit $Da \gg 1, Pe \gg 1$, the effective speed of the front is proportional to the area of the interface that separates the two phases. In two dimensions, the interface is characterized by its length, ℓ, and its depth, λ. We have the relationship $V_f \sim \lambda\ell/(L\tau_r)$ which entails the result that the ratio of the length of the interface in a moving medium, ℓ, to the length in a medium at rest, L, is $\ell/L \sim V_f/V_0$ and is therefore larger than unity. The structure responsible for this elongation of the front edge is the spiral wave shown in Figure 7.

Finally, it is interesting to look at the shape of the effective reaction term $\tau_{\text{eff}}^{-1}F(\Theta)$ appearing in the renormalized equation (32). As shown in Figure 9, for small Da the effective production term is indistinguishable from the "bare" one. Increasing Da, the reaction rate tends to reduce progressively, inducing the slow-down of the front speed. The effective potential shows a small region where the production term is essentially the microscopic one, followed by an intermediate regime characterized by a linear dependence on the cell-averaged concentration, with a slope directly proportional to Da^{-1}. That is in agreement with a typical effective reaction time $\tau_{\text{eff}} \sim \tau_r Da$ (cf. Eq. (34)).

We conclude the discussion on cellular flows by noting that the scaling behaviors V_f vs U are in agreement with the rigorous bounds $V_f \geq C_1 U^{1/5} + C_2$ and $V_f \geq C_3 U^{1/2} + C_4$ for slow and fast reaction [18].

C. Percolating Flow

In the previous subsections we discussed pure cellular and pure shear flows. Now we investigate the transition between these two limiting cases. To this aim, we will use for the lagrangian motion the generalized Harper map:

$$\begin{cases} x(t+1) = x(t) + U \sin y(t) \\ y(t+1) = y(t) + U_T \sin x(t+1) \mod 2\pi. \end{cases} \tag{36}$$

The case $U_T = 0$ corresponds to shear flow, whereas $U_T = U$ gives a chaotic cellular flow.

In order to give an idea of the Lagrangian behaviour of the flow generated by (36) we show in Fig. 10 some trajectories at different value of U_T. For $U_T \neq 0$ the map (36) exhibits chaotic behaviour in some regions. At small value of U_T one has basically a ballistic transport in the x direction apart from small recirculation regions. For $U_T \sim U$ a typical "cat's eye" pattern appears with percolating channels among the re-circulation regions. A chaotic cellular flow, rather similar to the case of convective cells discussed in section IV B (apart from a rotation of $\pi/4$) is obtained for $U_T = U$, see Fig. 10. The behaviour for $U_T \gg U$ can be understood by a simple statistical argument valid for large K [38]: at very large values of U_T, $y(t)$ changes very rapidly, therefore the oscillatory term $\sin(y(t))$ can be considered as a zero mean random process and the variable $x(t)$ is well approximated by a diffusive process with $D_{\text{eff}} \simeq U^2/4$.

In Fig. 11 we show snapshots of the concentration field for different reaction times. The natural question is how the transition from pure shear to percolation and from cellular flow to percolation, respectively, changes the front speed. On an intuitive basis we expect the front propagation to be slower in the cellular case than in the shear case. In Fig. 12 we plot the front speed in dependence of the sidewind U_T for different reaction time scales. The diffusion coefficient of the system (36) has been calculated in separate runs for the comparison with the homogeneization expectations.

Let us discuss the figure going from left to right, augmenting the sidewind. For zero sidewind, we recover the pure shear result, at the value $U_T = U$, we recover the pure cellular flow result and if we go even beyond, for a very large sidewind, the reaction becomes relatively small and thus we enter the homogeneization regime. This transition pure shear-pure cells is smooth as confirmed by the figure. The three horizontal lines show the asymptotic values of $2\sqrt{D_{\text{eff}}/\tau_r}$ (the value of D_{eff} does not change significantly as a function of U_T if U_T is large enough).

D. Final remarks

In the previous subsections we have shown the results for the behaviour of V_f as function of U and τ_r for different laminar flows discussing in detail the FKPP nonlinearity. It is natural to ask about the effects of the shape of $f(\theta)$ on the front speed V_f. In particular it is interesting to know whether the choice of an Arrhenius nonlinearity changes significantly the scenario presented in the previous sections.

It is known that for ignition nonlinearity, i.e. $f(\theta) = 0$ for $\theta < \theta_c$, and expectedly also in the Arrhenius case, the flow can suppress front propagation. This effect, called flame quenching, is absent for FKKP production terms. This observation may lead to the assumption that the front evolution could depend on the shape of $f(\theta)$ in a dramatic way. However, flame quenching takes place only if initial conditions of the field θ are localized, i.e. θ is different from zero only in a bounded region [6]. For the initial and boundary conditions that we use here (Eqs. (22)), the front propagates always [17,18], also in the Arrhenius case. For that reason, we do not expect major differences in the scaling properties of propagation speeds. Indeed, in the particular geometry we use, i.e. an open flow with an infinite reservoir of burned material, the values of V_f in the case of Arrhenius nonlinearity are very similar to the ones obtained using the FKPP nonlinearity. In Fig. 13 we show V_f as a function of U for the cellular flow introduced in Section IV B in the case of Arrhenius nonlinearity. The scaling laws $V_f \sim U^{1/4}$ and $V_f \sim U^{3/4}$ for slow and fast reaction hold also in this case. Also for shear and percolating flow we do not observe qualitative changes when varying the shape of $f(\theta)$.

Although the qualitative behaviour of V_f as a function of the system parameters does not change for different reaction terms, there are differences in the front speed relaxation to its asymptotic value. In the case of FKPP nonlinearity (i.e. "pulled" fronts), without advection ($\mathbf{u} = 0$), it is known [9] that the front velocity relaxes algebraically slow to its asymptotic value. Therefore one can expect some numerical difficulties to find out the value of V_f, in particular for the slow reaction case in which the front may interest a very large spatial

region. With this "caveat" in mind, in our simulations we varied the system size to carefully check the convergence of V_f. Using Arrhenius nonlinearity (i.e. "pushed" front) in the case without advection is known that the convergence to the asymptotic value is exponentially fast. Also in presence of a velocity field we observe that the convergence is much faster than in the FKPP case.

V. SUMMARY AND CONCLUSIONS

Enhancement of front propagation by an underlying flow is a generic phenomenon for advection-reaction-diffusion systems. A relevant question is how the front speed V_f depends on the detailed properties of the advecting velocity field, in particular on the typical velocity U. For an arbitrary flow, it is extremely difficult to derive this dependence analytically. Here, we have shown that for all incompressible flows there exists an upper bound to the front speed that links it to a single global property of the flow, its effective diffusion coefficient. The analytic derivation of the effective diffusivity for a given velocity field is itself a daunting task, but several generic properties are known and some exact results are available for simple flows. In the special case of fast advection, as compared to the reaction timescale τ_r, the upper bound is sharp, and therefore it is possible to obtain the dependence of V_f on U. When molecular diffusivity is small we have $V_f \sim U$ for flows with open streamlines such as the shear flow, and $V_f \sim U^{1/4}$ for cellular flows. For slow advection, the bound ceases to be effective, and one has to resort to numerical simulations in order to determine the front speed. We find that for open-streamline flows there is still a linear dependence $V_f \sim U$ whereas cellular flows display a $V_f \sim U^{3/4}$ dependence. Within the class of initial/boundary conditions for which no flame quenching effect ever takes place, those scaling laws appear to be universal with respect to the details of the reaction mechanism.

Which lessons can we draw from the present results for the open, challenging problem of front propagation in turbulent flows? The main point that we want to emphasize is the central role played by the effective diffusion process in determining the front speed. That

is a reflection of the deep-rooted link between front propagation and transport properties. The knowledge of turbulent transport has experienced a significant progress in the past few years (see e.g. Refs [39] and [40]). We believe that those results will reveal helpful to shed light on the issue of front propagation in turbulent flow (for a similar point of view, see Ref. [41]).

VI. ACKNOWLEDGMENTS

APPENDIX A: HOMOGENIZATION REGIME

In this appendix we present briefly the application of homogenization techniques [42] to the reaction-advection-diffusion equation (1). We are interested in the large-time, large-scale asymptotics for slow reaction timescales. Introducing the small parameter ϵ, we consider reaction times $\tau_r = \bar{\tau}_r \epsilon^{-2}$, and look at the solutions of Eq. (1) for times $O(\epsilon^{-2})$ and scales $O(\epsilon^{-1})$. The separation in time-scales allows a multi-scale treatment. Slow variables $\mathbf{X} = \epsilon \mathbf{x}$ and $T = \epsilon^2 t$ are introduced along with the fast variables $\mathbf{x}$ and t. Slow and fast variables are considered as being independent. As a consequence space-derivatives act as $\partial_x + \epsilon \partial_X$ and the time-derivative as $\partial_t + \epsilon^2 \partial_T$. The concentration field is expanded in a power series in ϵ as $\theta(\mathbf{x}, t, \mathbf{X}, T) = \theta^{(0)}(\mathbf{x}, t, \mathbf{X}, T) + \epsilon \theta^{(1)}(\mathbf{x}, t, \mathbf{X}, T) + \ldots$, and this expression is plugged in Eq. (1). At zero-th order in ϵ the equation reads

$$\partial_t \theta^{(0)} + \mathbf{u} \cdot \nabla_x \theta^{(0)} = D_0 \nabla_x^2 \theta^{(0)} \ .$$

Due to the dissipative nature of the latter equation, the solution at zero-th order will decay to its average value on fast timescales:

$$\theta^{(0)}(\mathbf{x}, t, \mathbf{X}, T) = \theta^{(0)}(\mathbf{X}, T) \ .$$

At order ϵ, we obtain the linear equation

$$\partial_t \theta^{(1)} + \mathbf{u} \cdot \nabla_x \theta^{(1)} - D_0 \nabla_x^2 \theta^{(1)} = -\mathbf{u} \cdot \nabla_X \theta^{(0)}$$

which allows the solution

$$\theta^{(1)}(\mathbf{x}, t, \mathbf{X}, T) = \theta^{(1)}(\mathbf{X}, T) + \mathbf{w}(\mathbf{x}, t) \cdot \nabla_X \theta^{(0)}(\mathbf{X}, T) \ ,$$

provided that the auxiliary field $\mathbf{w}$ obeys the equation

$$\partial_t \mathbf{w} + \mathbf{u} \cdot \nabla_x \mathbf{w} = D_0 \nabla_x^2 \mathbf{w} - \mathbf{u} \ .$$

Remark that the production term has not shown up yet. It is at order ϵ^2 that it enters the scene

$$\partial_t \theta^{(2)} + \mathbf{u} \cdot \nabla_x \theta^{(2)} - D_0 \nabla_x^2 \theta^{(2)} = -\partial_T \theta^{(0)} - \mathbf{u} \cdot \nabla_X \theta^{(1)} + D_0 \nabla_X^2 \theta^{(0)} +$$

$$2 D_0 \nabla_x \cdot \nabla_X \theta^{(1)} + \frac{1}{\bar{\tau}_r} f(\theta^{(0)}) \ .$$

The solvability condition for the equation at second order requires that

$$\partial_T \theta^{(0)} = D_0 \nabla_X^2 \theta^{(0)} - \langle \mathbf{u} \cdot \nabla_X \theta^{(1)} \rangle + \frac{1}{\bar{\tau}_r} f(\theta^{(0)})$$

where the brackets denote the average over the fast variables. Plugging the expression for $\theta^{(1)}$ into the solvability condition yields the effective, large-scale equation

$$\partial_T \theta^{(0)} = \sum_{i,j} D_{\text{eff}}^{ij} \partial_{X^i X^j}^2 \theta^{(0)} + \frac{1}{\bar{\tau}_r} f(\theta^0)$$

where D_{eff} is in general a tensor with components $D_{\text{eff}}^{ij} = D_0 \delta^{ij} - \frac{1}{2} \langle u^i w^j + u^j w^i \rangle$. Considering the propagation in the x-direction only, we recover an effective equation which is equivalent to Eq. (1) with an effective diffusivity. Therefore the front propagates at a maximal speed (computed in the original, fast variables) given by $V_f \leq 2 \sqrt{\frac{D_{\text{eff}}}{\tau_r} \left(\sup_\theta \frac{f(\theta)}{\theta} \right)}$, for FKPP nonlinearity one has $V_f = 2\sqrt{\frac{D_{\text{eff}}}{\tau_r}}$, where $D_{\text{eff}} = D_{\text{eff}}^{11}$.

APPENDIX B: FRONT SPEED FOR DISCRETE TIME MAPS

The front speed (25) for discrete maps can be obtained by simple considerations just following the standard way used for the derivation of V_f in the continuous time limit:

$$\frac{\partial}{\partial t}\theta = D_0 \nabla^2 \theta + \frac{1}{\tau_r} f(\theta) \ . \tag{B1}$$

Let us consider a front propagating from left to right. For the sake of simplicity we discuss a FKPP nonlinearity for the one dimensional case. For $x \to \infty$, $\theta(x,t)$ has an exponential shape,

$$\theta(x,t) = e^{at-bx} \ , \tag{B2}$$

up to exponentially subleading terms. Inserting (B2) in (B1) and linearizing around $\theta = 0$ one has:

$$a = D_0 b^2 + \frac{1}{\tau_r} f'(0) \ . \tag{B3}$$

A saddle point argument gives a selection criterion which allows for the determination of the front speed [9]:

$$V_f = \min_b \frac{a(b)}{b} = 2\sqrt{\frac{D_0}{\tau_r} f'(0)} \ . \tag{B4}$$

Consider now the discrete time reaction case, i.e.:

$$\frac{\partial}{\partial t}\theta = D_0 \nabla^2 \theta + \sum_{n=-\infty}^{\infty} g(\theta)\delta(t-n) \ , \tag{B5}$$

where for sake of simplicity we adopt $\Delta t = 1$ (see Eq. (14)).
Indicating with $G(\theta)$ the reaction map (see Eq. (15)) one has:

$$\theta(x,t+0) = G(\theta(x,t-0)) \ .$$

Integrating the diffusion equation $\partial_t \theta = D_0 \nabla^2 \theta$ between $t+0$ and $t+1-0$ one has:

$$\theta(x,t+1-0) = \frac{1}{\sqrt{2\pi}} \int e^{-\frac{w^2}{2}} G\left(\theta(x-\sqrt{2D_0}\,w,t+0)\right) dw \ , \tag{B6}$$

Assuming the shape (B2) and linearizing around $\theta = 0$, i.e.: $G(\theta) \simeq G'(0)\theta$, a simple gaussian integration gives:

$$e^{a(t+1)-bx} \sim e^{\ln G'(0)+D_0 b^2 - bx + at} \ .$$

The above result implies

$$a = \ln G'(0) + D_0 b^2$$

this is nothing but Eq. (B3) now with $\ln G'(0)$ instead of $\frac{1}{\tau_r} f'(0)$. The same selection criterion gives

$$V_f = 2\sqrt{D_0 \ln G'(0)} \ . \tag{B7}$$

APPENDIX C: NUMERICAL METHOD

Since we are interested in propagation along the x-axis, we consider a slab with sides $L_x \gg L_y$. The boundary conditions are periodic in the y-direction $\theta(x, y, t) = \theta(x, y + L_y, t)$. To fulfill the conditions (22) $\lim_{x \to \infty} \theta(x, y, t) = 0$ and $\lim_{x \to -\infty} \theta(x, y, t) = 1$ numerically, we set $\theta(0, y, t) = 1$ and $\theta(L_x, y, t) = 0$, which is a good approximation as long as the fronts leading edge has not reached L_x. We introduce a lattice of step size Δx and Δy (for sake of simplicity we assume $\Delta x = \Delta y$) so that the field $\theta(x, y, t)$ is defined on the points $\mathbf{x}_{n,m} = (n\Delta x, m\Delta y)$. The numerical code computes $\theta_{n,m}(t + \Delta t) = \theta(n\Delta x, m\Delta y, t + \Delta t)$ in terms of $\theta_{n,m}(t)$ using Eq. (16). For each grid point $\mathbf{x}_{n,m}$, one introduces N independent standard gaussian variables $\mathbf{W}^\alpha$, $\alpha = 1, \ldots, N$, $N \gg 1$, and computes $\tilde{\mathbf{x}}_{n,m}^\alpha = \mathbf{x}_{n,m} - \sqrt{2D_0 \Delta t}\, \mathbf{W}^\alpha$ and finally from this $\mathbf{r}_{n,m}^\alpha = \mathbf{F}^{-1}(\tilde{\mathbf{x}}_{n,m}^\alpha)$. For $\theta_{n,m}(t + \Delta t)$ one needs the values of θ at time t in the positions $\mathbf{r}_{n,m}^\alpha$. In general the $\mathbf{r}_{m,n}^\alpha$ are not on the grid points $(n\Delta x, m\Delta y)$, nevertheless we can compute the value $\theta(\mathbf{r}_{n,m}^\alpha, t)$ using linear interpolation from $\theta_{n,m}(t)$. Therefore we have

$$\theta_{n,m}(t + \Delta t) = \frac{1}{N} \sum_{\alpha=1}^{N} G[\theta(\mathbf{r}_{n,m}^\alpha, t)]. \tag{C1}$$

Typically one has a good convergence for $N = 50$. To simulate the diffusion process we have to impose a relation between D_0, Δx and Δt to insure that the diffusion transports a particle over distances larger than the grid-size, $\frac{\sqrt{2D_0 \Delta t}}{\Delta x} > 1$ (see Fig 14).

REFERENCES

[1] F. A. Williams, *Combustion Theory*, Benjamin-Cummings, Menlo Park (1985); E. R. Abraham, Nature **391**, 577 (1998); I. R. Epstein, Nature **374**, 231 (1998); J. Ross, S. C. Müller, and C. Vidal, Science **240**, 460 (1988).

[2] N. Peters, *Turbulent Combustion*, Cambridge Univ. Press, Cambridge UK (2000).

[3] S. Malham and J. Xin, Comm. Math. Phys **199**, 287 (1998).

[4] A. N. Kolmogorov, I. G. Petrovskii, and N. S. Piskunov, Moscow Univ. Bull. Math. **1**, 1 (1937); R. A. Fischer, Ann. Eugenics **7**, 355 (1937).

[5] J. Xin, SIAM Review **42**, 161 (2000).

[6] P. Constantin, A. Kiselev and L. Ryzhik, LANL e-print archive nlin/0006024 (2000).

[7] D. G. Aronson and H. F. Weinberg, Adv. Math. **30**, 33 (1978).

[8] J. Armero, A. Lacasta, L. Ramirez-Piscina, J. Casademunt, J. M. Sancho and F. Sagues, Phys Rev E **56**, 5405 (1997).

[9] U. Ebert and W. Van Saarloos, Physica D **146**, 1 (2000).

[10] P. Clavin, and F. A. Williams, J. Fluid Mech. **90**, 589 (1979).

[11] A. R. Kerstein, and W. T. Ashurst, Phys. Rev. Lett **68**, 934 (1992).

[12] M. N. Rosenbluth, A. L. Berk, I. Doxas, and W. Horton, Phys. Fluids **30**, 2636 (1987).

[13] B. I. Shraiman, Phys. Rev. A **36**, 261 (1987).

[14] Y. Pomeau C. R. Acad. Sci. **301**, 1323 (1985).

[15] P. B. Rhines and W. R. Young, J. Fluid Mech. **133**, 133 (1983).

[16] P. D. Ronney, in *Modeling in Combustion Science* 3, Eds. J. Buckmaster and T. Takeno (Springer, New York 1995).

[17] P. Constantin, A. Kiselev, A. Oberman, and L. Ryzhik, LANL e-print archive math/9907132 (1999).

[18] A. Kiselev and L. Ryzhik, LANL e-print archive math/0002175 (2000).

[19] R. M. McLaughlin and J. Zhu, Comb. Sci. and Tech. **129**, 89 (1997).

[20] P. F. Embid, A. Majda and P. E. Sounganidis, Phys. Fluids **7**, 2052 (1995).

[21] U. Yakhot, Comb. Sci. and Tech. **60**, 191 (1988).

[22] A. Pocheau, Phys. Rev. E **49**, 1109 (1994).

[23] A. C. Martí, F. Sagues and J. M. Sancho, Phys. Fluids **9**, 3851 (1997).

[24] H. Aref, J. Fluid Mech. **143**, 1 (1984); J. M. Ottino, Ann. Rev. Fluid Mech. **22**, 207 (1990); A. Crisanti, M. Falcioni, G. Paladin and A. Vulpiani, La Rivista del Nuovo Cimento **14** (12), 1 (1991).

[25] M. Freidlin, *Markov Processes and Differential Equations* Birkhauser, Boston (1996).

[26] S. Fedotov, Phys. Rev. E **55** 2750 (1997).

[27] M. Avellaneda, and A. Majda, Phys. Rev. Lett. **62**, 753 (1989).

[28] P. Castiglione, A. Crisanti, A. Mazzino, M. Vergassola and A. Vulpiani, J. Phys. **A 31**, 7197 (1998).

[29] G. M. Zaslavsky, D. Stevens and H. Weitzner, Phys. Rev. E **48**, 1683 (1993).

[30] Ya. B. Zel'dovich, Sov. Phys. Dokl. **27**, 797 (1982).

[31] N. Vladimirova, F. Cattaneo, A. Malagoli, A. Oberdam and O. Ruchayskiy, preprint 2000.

[32] M. Avellaneda and M. Vergassola Phys. Rev. E **52**, 3249 (1995).

[33] R. H. Kraichnan, in *The Padé Approximants in Theoretical Physics*, Acad. Press Inc.,

New York (1970).

[34] G. I. Taylor, Proc. London Math. Soc. **20**, 196 (1921).

[35] A. J. Majda, and P. R. Kramer, Phys. Rep. **314**, 237 (1999).

[36] B. Audoly, H. Beresytcki and Y. Pomeau C. R. Acad. Sci. **328**, Série II b, 255 (2000).

[37] P. D. Ronney, B. D. Haslam and N. O. Rhys, Phys. Rev. Lett. **74**, 3804 (1995).

[38] A. J. Lichtenberg and M. A. Liebermann, *Regular and Chaotic Dynamics* (Springer-Verlag, Berlin 1992).

[39] B. Shraiman and E. Siggia, Nature **405**, 639 (2000).

[40] G. Falkovich, K. Gawędzki and M. Vergassola, Rev. Mod. Phys., in press. (2001).

[41] M. Chertkov and V. Yakhot, Phys. Rev. Lett. **80** , 2837 (1998).

[42] A. J. Majda and P. R. Kramer, Phys. Rep. **314**, 237 (1999); A. Bensoussan, J. Lions and G. Papanicolaou *Asymptotic Analysis for Periodic Structures* (North Holland, Amsterdam 1978).
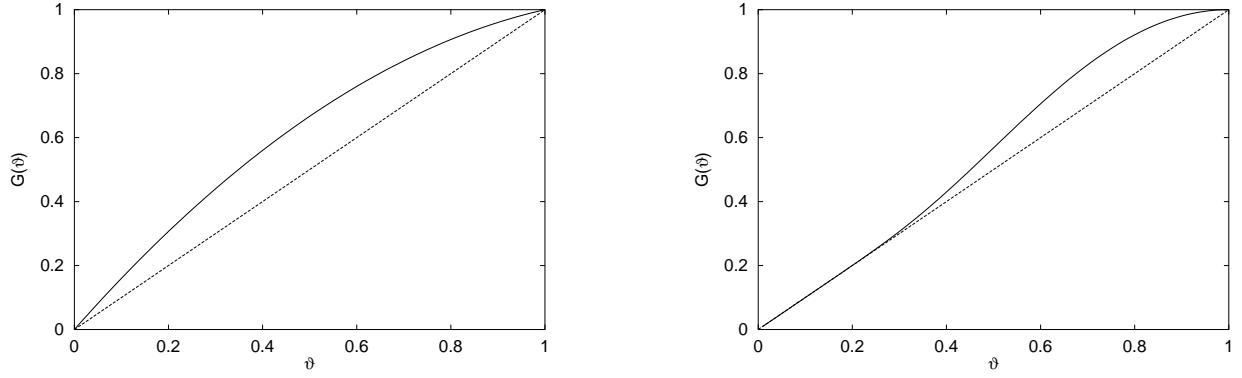
FIG. 1. Two examples of reaction maps. On the left FKPP type, on the right Arrhenius type.
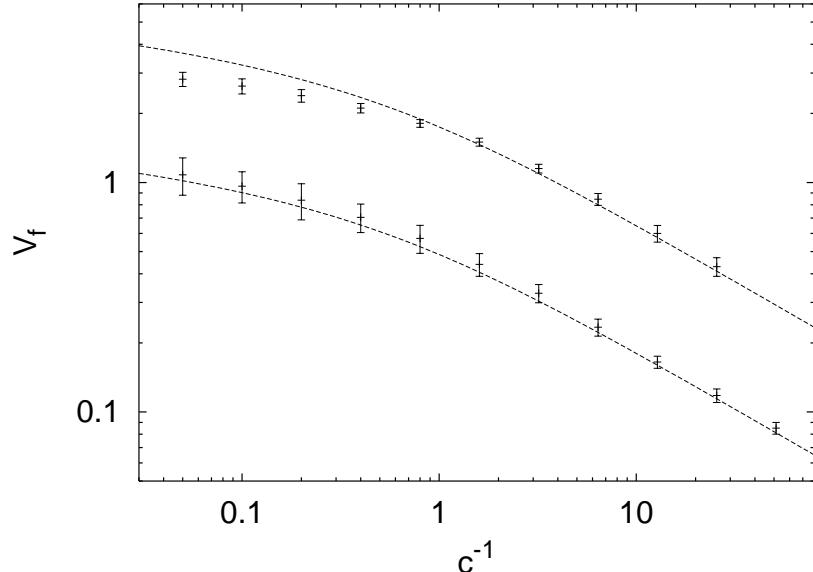
FIG. 2. Front speed for the standard map (28) with reaction map given by Eq. (29) (30), as function of c, $D_0 = 0.04$. The upper curve is for $K = 3.0$, the lower for $K = 1.0$. The dotted lines are the homogenization curves $2\sqrt{D_{\text{eff}} \ln(1.0 + c)}$. The diffusion coefficient D_{eff} depends on K and has been computed numerically.

FIG. 3. Snapshots of the field $\theta(x, y)$ for the shear map (31) and the reaction map (29,30). $U = 0.5$, $D_0 = 0.01$, $c = 0.2$ and $c = 2.0$ for the upper and lower image respectively. The system size is $L_y = 2\pi$ and $L_x = 20\pi$.
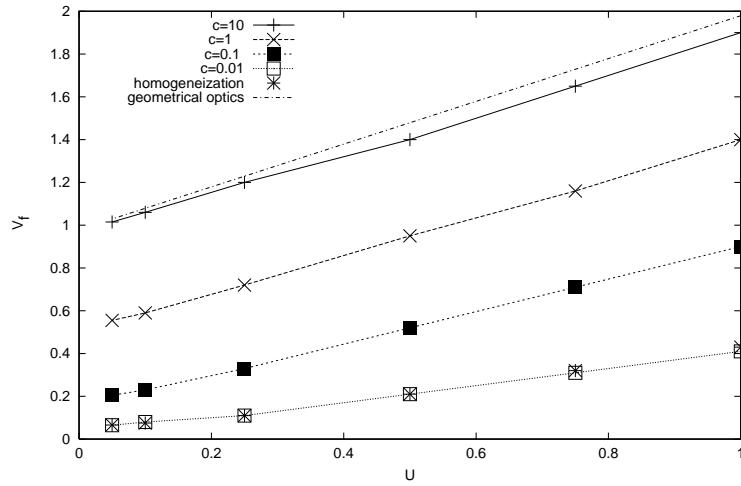
FIG. 4. Front speed for the shear map (31) and the reaction map (29, 30) as function of U for various reaction times $\tau_r = \frac{1}{\ln(1+c)}$, $D_0 = 0.04$.
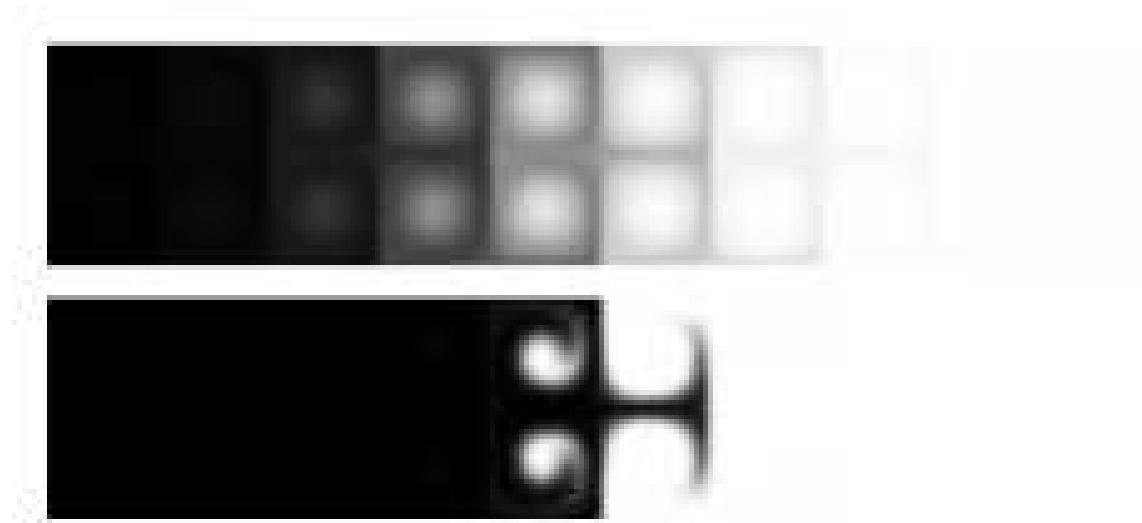
FIG. 5. Snapshots of the field $\theta(x, y)$ for cellular flow given by the streamfunction (20) and the reaction map (29, 30), $U = 2.0$, $D_0 = 0.01$, $\tau_r = 5.0$ and $\tau_r = 0.5$ for the upper and lower image respectively. The system size is $L_y = 2\pi$ and $L_x = 10\pi$.
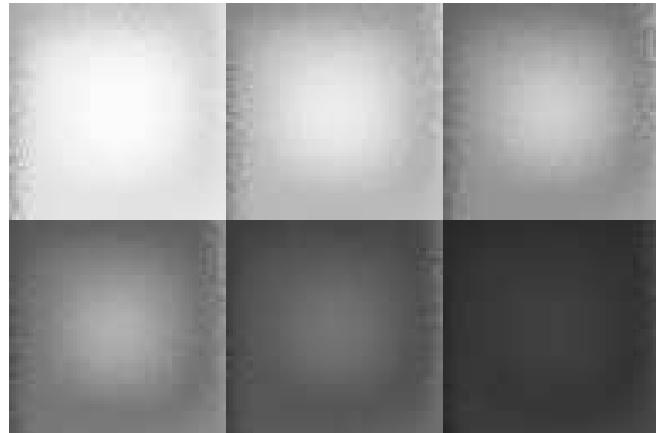
FIG. 6. Cellular flow: six snapshots of the field θ within the same cell, at six successive times with a delay $\tau/6$ (from left to right, top to bottom), as a result of the numerical integration of equation (1). Here $Da \simeq 0.4$, $Pe \simeq 315$. Black stands for $\theta = 1$, white for $\theta = 0$.
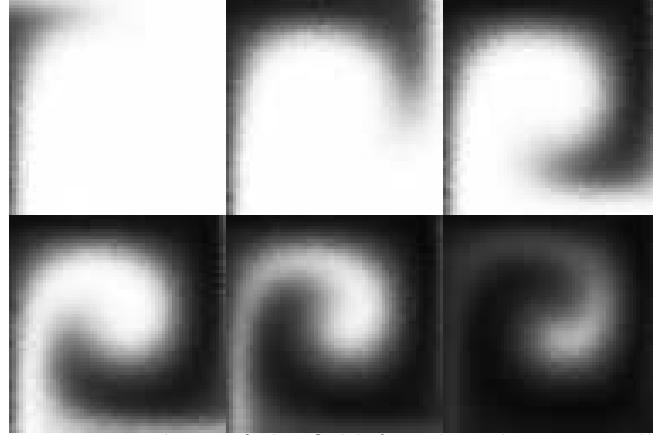
FIG. 7. Cellular flow: six snapshots of the field θ within the same cell, at six successive times with a delay $(L/U)/6$ (left to right, top to bottom). Here $Da = 4, Pe = 315$. A spiral wave invades the interior of the cell, with a speed comparable to U.
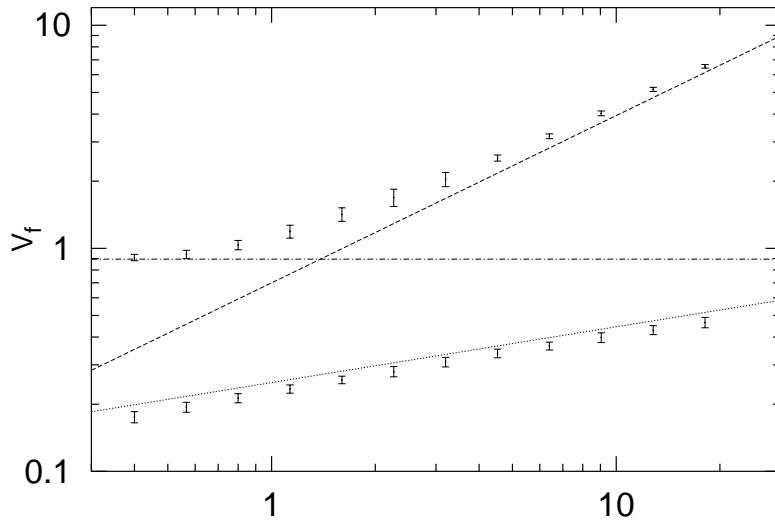
FIG. 8. Cellular flow: the front speed V_f as a function of U, the typical flow velocity, with $D_0 = 0.04$. The lower curve shows data at $\tau_r = 20.0$ (fast advection). The upper curve shows data at $\tau_r = 0.2$ (slow advection). For comparison, the scalings $U^{1/4}$ and $U^{3/4}$ are shown as dotted and dashed lines respectively. The horizontal line indicate V_0 (the front speed without advection, i.e. $U = 0$) for $\tau_r = 0.2$.

34
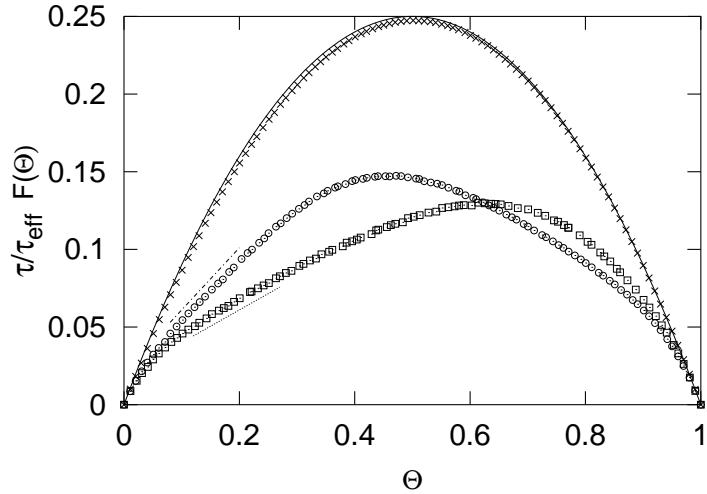
FIG. 9. Cellular flow: the renormalized reaction term $\tau_r/\tau_{\text{eff}} F(\Theta)$ vs Θ for three different parameters: $Da \simeq 4$ ($\square$), $Da \simeq 2$ ($\circ$) and $Da \simeq 0.4$ ($\times$). The continuous line is $f(\theta)$. The dotted and dash-dotted lines have the slopes (0.2 and 0.4) proportional to Da^{-1} in the region of slow advection.
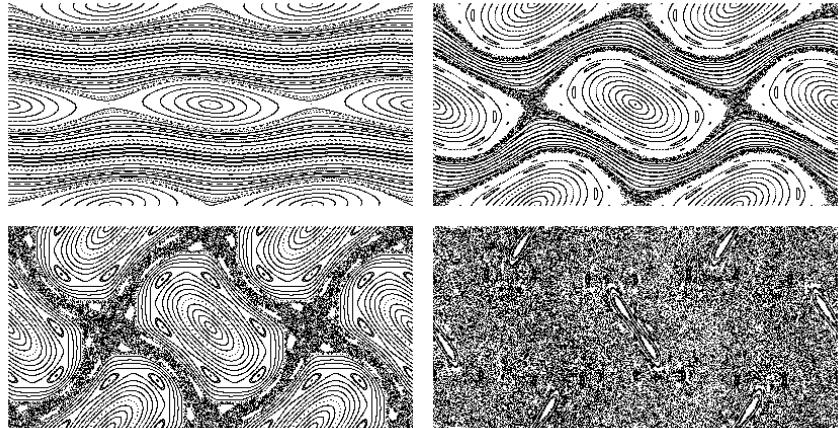

FIG. 10. Lagrangian dynamics of test particles evolving according to the Harper's map (36) for different values of U_T, with $U = 1.5$. From top-left moving clockwise: $U_T = 0.2$, $U_T = 0.8$, $U_T = 1.5$ and $U_T = 3.0$.

35
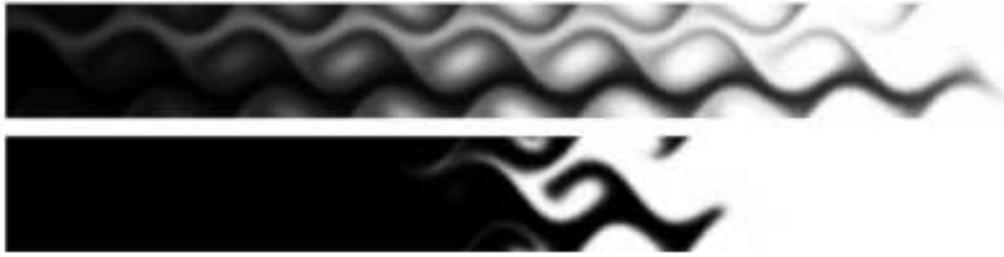
FIG. 11. Snapshots of the field $\theta(x, y)$ for percolating flow given by Eq. (36). The reaction map is given by (29,30). $U = 1.5$, $U_T = 0.8$, $D_0 = 0.01$, $c = 0.2$ and $c = 2.0$ for the upper and lower image respectively. The system size is $L_y = 2\pi$ and $L_x = 20\pi$.
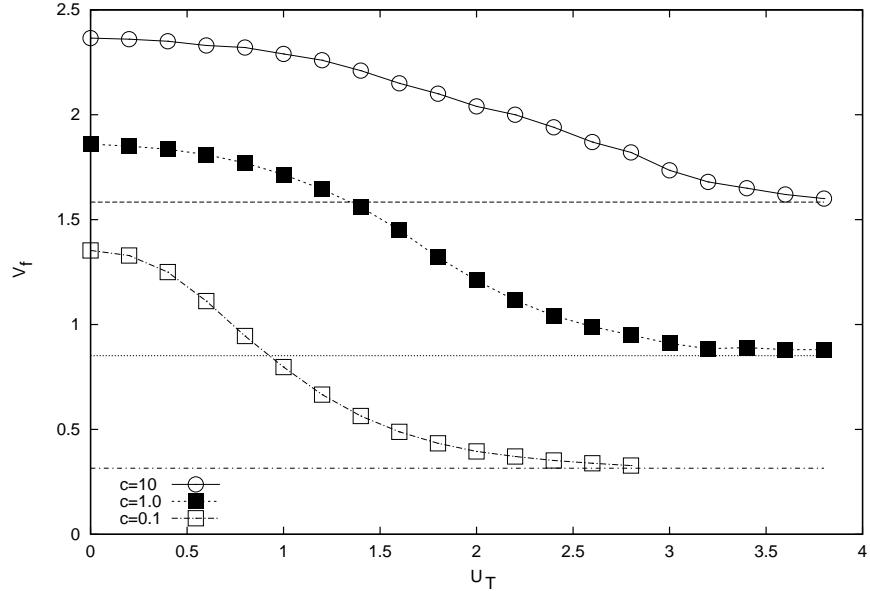

FIG. 12. V_f vs U_T, the Lagrangian map is given by (36), the reaction map $G(\theta)$ is given by (29,30). The three curves correspond to $c = 0.1, 1.0, 10.0$ (from bottom to top), the "horizontal" velocity has been fixed to $U = 1.5$ for all curves. The asymptotic value of $2\sqrt{D_{\mathrm{eff}} \ln(1 + c)}$ (for the horizontal direction) is shown by the three horizontal lines, the corresponding value of D_{eff} has been calculated numerically for large U_T.
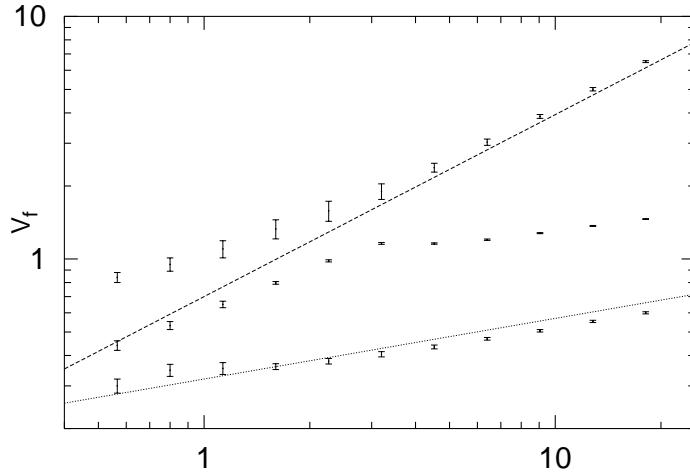
FIG. 13. Cellular flow: the front speed V_f as a function of U, the typical flow velocity in the case of Arrhenius production type: $f(\theta) = (1 - \theta)\exp(-\theta_c/\theta)$. The lower curve shows data at $\tau_r = 2.0$ and $\theta_c = 0.5$ (fast advection). The intermediate curve at $\tau_r = 2.0$ and $\theta_c = 0.2$ shows the crossover from fast (right side) to slow advection (left side). The upper curve shows data at $\tau_r = 0.2$ and $\theta_c = 0.2$ (slow advection). For comparison, the scalings $U^{1/4}$ and $U^{3/4}$ are shown as dotted and dashed lines respectively.
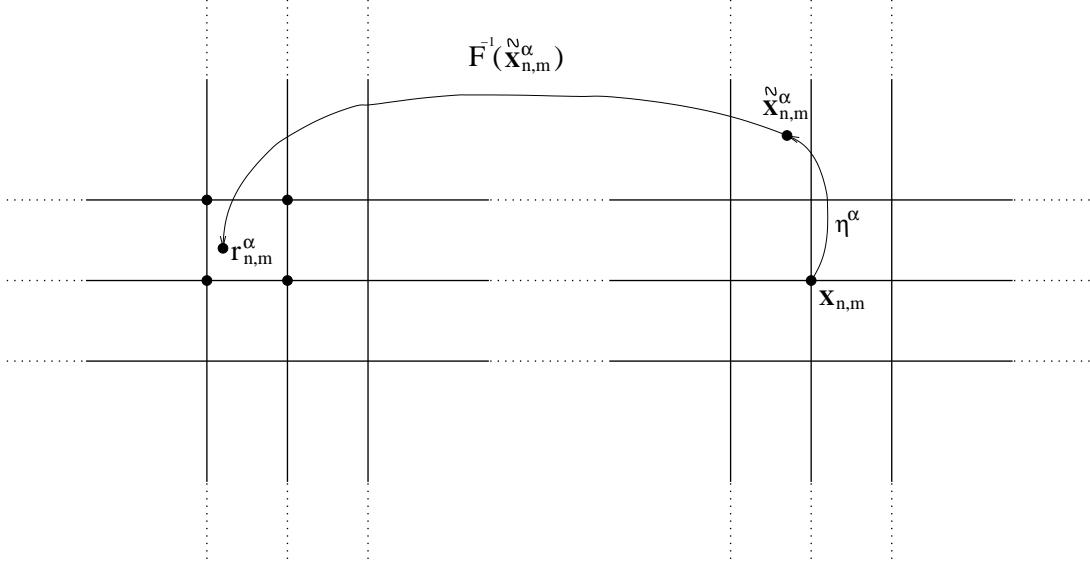

FIG. 14. Pictorial scheme of the numerical algorithm, as discussed in Appendix C. Here, $\eta^\alpha = \sqrt{2D_0\,\Delta t}\,\mathbf{W}^\alpha$ where $\mathbf{W}^\alpha$ is a standard gaussian variable.